J. Heat Treat. (1989) 7:107–121

Determination of the Local Quench Curve for Spray-Cooled Metallic Surfaces

I. Mudawar and W.S. Valentine

Abstract. An experimental study of heat transfer from hot metallic surfaces to water sprays was conducted in the single-phase, nucleate boiling, and transition boiling regimes of the quench curve for surface temperatures below 400° C. Heat transfer measurements were made locally in the spray field using a heater surface area of 0.5 cm^2. The hydrodynamic properties of the sprays such as drop diameters, drop velocities, and volumetric spray flux were also measured independently at a position in the spray field identical to that of the heater. The test conditions included variations in volumetric spray flux, mass mean drop diameter, and mean drop velocity of 0.6×10^{-3} to 9.96×10^{-3} m^3s^{-1}/m^2, 0.434 to 2.005 mm, and 10.6 to 26.5 m/s, respectively. Correlations are presented for water temperatures from 23 to 80° C. These correlations constitute a universal approach to the development of quench curves for industrial sprays commonly employed in materials processing.

NOMENCLATURE

CHF = critical heat flux
C = constant
c_p = specific heat at constant pressure
d = drop diameter (m)
h = heat transfer coefficient, $q''/(T_{sur} - T_f)$ (W/m^2K)
h_{fg} = latent heat of vaporization (J/kg)
k = thermal conductivity (W/m K)
L = characteristic length (m)
n_i = number of drops of diameter d_i in a spray sample
N = total number of drops in a spray sample
Nu = Nusselt number, hd/k_f
P = pressure (Psi)
Pr = Prandtl number
q'' = heat flux (W/m^2)
Q'' = volumetric spray flux (m^3s^{-1}/m^2)
Re = Reynolds number ($Q''d/\nu_f$)
T = temperature (K)
ΔT_{sat} = surface superheat, $(T_{sur} - T_{sat})$(° C)
ΔT_{sub} = degree of subcooling, $(T_{sat} - T_f)$(° C)
u = velocity (m/s)
U = characteristic velocity (m/s)
x_i = number of drops of diameter d_i crossing a unit transverse surface area per unit time
X = total number of drops crossing a unit transverse surface area per unit time.

Greek Symbols

ν = kinematic viscosity (m^2/s)
ρ = density (kg/m^3)
σ = surface tension (N/m)

Subscripts

d = drop
f = liquid
g = vapor
$Leid$ = Leidenfrost
m = mean
max = CHF
sat = saturation
sub = subcooling
sur = surface

I. Mudawar is Associate Professor and Director of the Boiling and Two-Phase Flow Laboratory and W.S. Valentine is a Graduate Research Assistant at Purdue University, West Lafayette, IN 47907, USA.

INTRODUCTION

Manufacture of alloys requires efficient control of many interdependent processes such as hot working, an-

nealing, and controlled heating and cooling. These processes all influence the internal structure of the alloy and hence, control the final properties. Cost-effective fabrication of heat treated alloys such as aluminum has led to the development of "press quenching" for the final cooling step of extrusions. During press quenching, the alloy is cooled by a deluge of water sprays immediately after exiting the die. Improper cooling can cause insufficient aging, warpage, nonuniformity of properties, and surface fracture. Presently, a method for accurately determining spray nozzle position and flow rate is not available. Consequently, after press quenching, a costly post treatment consisting of additional heat treatment and manual straightening of warped shapes is required to meet product specifications.

It is estimated that 50% of the cost of post treatment of aluminum extrusions is due to stresses thermally induced during the press quenching process. Therefore, in order to improve quality and consistency between production runs and to reduce cost, a method for optimizing the cooling rate for a particular shape and material is needed. The present project constitutes the first step in the development of a new intelligent quenching technology currently being examined at Purdue's Boiling and Two-Phase Flow Laboratory [1]. The proposed technology consists of incorporating robotics, sensors, etc., into press quenching technology, and involves synthesis via CAD/CAM of heat transfer and materials engineering. As shown in Figure 1, with the proposed technology, an operator could input to a CAD system the geometry and desired properties of the product. The intelligent system would output the proper spray nozzle locations and flow rates needed to accomplish the desired results. Possibly, the CAD system could robotically control spray nozzle positions and flow rates. The first step in developing this semi-expert system is to understand the dynamics of thermal interaction between sprayed drops and hot surfaces.

When a preheated metallic surface is quenched, its surface experiences four distinct heat transfer regimes which can be traced along the "boiling curve." As shown in Figure 2, the boiling curve is a plot of surface heat flux versus excess surface temperature above saturation. When a preheated alloy exits the die in an extrusion, forging, or continuous casting process, it is typically at a temperature above the Leidenfrost point and the surface experiences film boiling. This boiling regime is characterized by a thermally-insulating layer of steam forming between the surface and individual impinging drops, resulting in poor heat transfer. When the Leidenfrost temperature is reached, the vapor film is interrupted by partial contact of liquid with the surface, causing the surface heat flux to increase with decreasing temperature until the point of critical heat flux (CHF). After CHF, the surface is cooled by nucleate boiling until the temperature falls into the single-phase regime. Spray cooling is preferred to quenching in stagnant liquid because it raises the Lei-

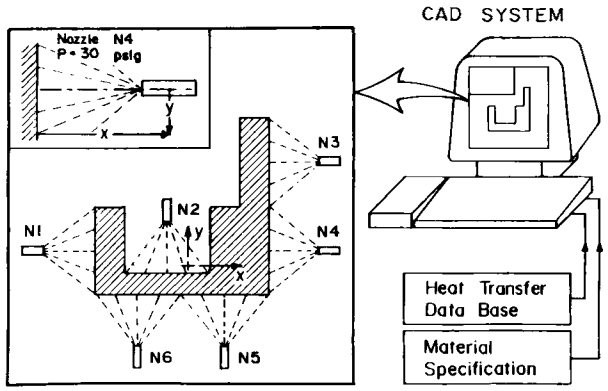

Fig. 1. Schematic representation of the semi-expert spray cooling technology.

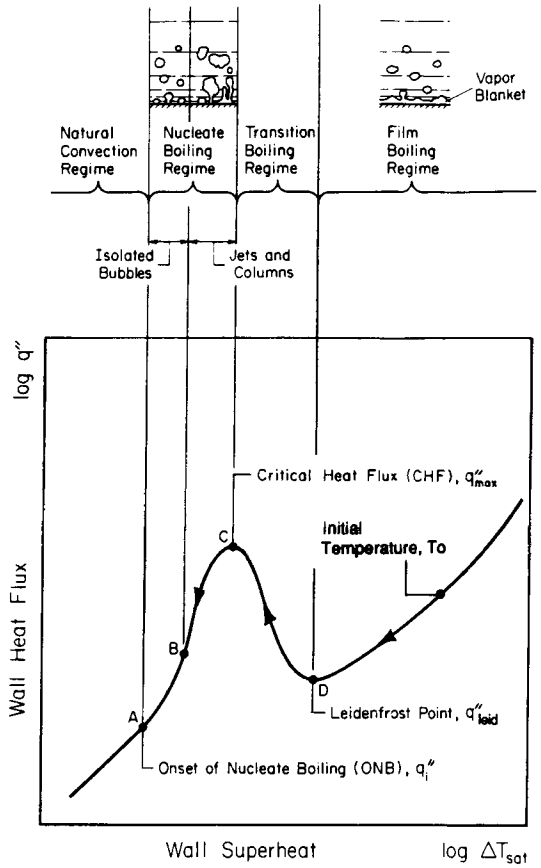

Fig. 2. Boiling curve associated with quenching of a hot surface in a stagnant pool of liquid at saturation temperature.

denfrost temperature and enhances significantly the heat transfer rate even in the film boiling regime.

The precise shape of the quench (or boiling) curve is dependent upon several parameters such as water temperature, surface roughness, and spray hydrodynamics. For example, an increase in surface roughness, mean drop velocity, or volumetric spray flux can increase the Leidenfrost temperature. While the effects of these parameters are not well understood, it is known that their combined effect can increase the Leidenfrost temperature from 350 to 900°C [2]. Such an increase could totally eliminate the film boiling regime for many quenching processes, especially for aluminum alloys.

Unfortunately, the spray boiling curve is not well defined especially for the transition, nucleate, and single-phase regimes. Most research in the past has been limited to spray cooling in the film boiling regime at high temperatures applicable to the quenching of steel.

After conducting a review of literature on heat transfer to sprays in the film boiling regime, Brimacombe et al. [3] concluded that the heat transfer rate is proportional to the volumetric spray flux, Q'', to some power between 0.5 and 1.0. While authors agree that Q'' is the dominant spray parameter [2–16], there is no convincing evidence that it is the only parameter with a noticeable effect on heat transfer. Urbanovich et al. [15], for example, showed that heat transfer is a function of Q'', the pressure difference at the nozzle, and location within the spray field. It is well known that atomization of pressure sprays results in a wide spectrum of drops having different diameters, velocities, and trajectories. These hydrodynamic characteristics are strongly influenced by nozzle pressure drop. The dependence of heat transfer on nozzle pressure drop suggests the distributions of drop diameters and velocities through the spray influence heat transfer.

Spatial nonuniformity of cooling through the spray field, which is possibly due to nonuniform distributions of drop diameters and velocities, has been demonstrated by Reiners et al. [12] who found the convection coefficient to vary significantly over short distances. Studies by Hoogendoorn and den Hond [2] and Bolle and Moureau [4,5] showed minimal influence of spray orientation with respect to the heated surface, suggesting heat transfer to a spray is determined by initial impact of the drops and not the runoff flow on the surface following impact. Their observations add credibility to studies based on local heat transfer measurements.

Hoogendoorn and den Hond found that, by changing spray conditions, it is possible to vary the Leidenfrost temperature over a range from 350 to 900°C, proving that the spray boiling curve is highly sensitive to spray characteristics. Unlike steel making, spray quenching of some alloys such as aluminum takes place at surface temperatures below 480°C. Consequently, the entire quenching process may take place below the Leidenfrost temperature where little study and almost no useful heat transfer correlations are available.

The overall goal of this experimental study is to provide metal industries with a universal data base for the design and operation of spray quenching systems. This data base would be used to predict the heat transfer characteristics of a spray of known hydrodynamic properties. More specifically, the study focuses on obtaining local heat transfer measurements in spray fields to simulate local quench characteristics of metallic surfaces below 400°C. This includes the development of heat transfer correlations for the various regimes of the spray boiling curve.

EXPERIMENTAL FACILITY

Flow Loop

The experimental facility consisted of a test heater, which simulated a quenched alloy, and a flow loop designed to deliver spray fluid at the desired conditions. Except for the test chamber, which was made of paper phenolic, the fluid was circulated through stainless steel plumbing components. Up to 30 gallons of water stored at the lower section of the test chamber were preheated by a 4000 Watt immersion heater as shown in Figure 3. The water was pumped from the reservoir via a stainless steel rotary vain pump which delivered up to 4.45 gpm at 100 psi. Further temperature control of the fluid was achieved by an inline electric preheater or a water-cooled plate-type heat exchanger, depending upon the operating temperature of the water. Downstream from the heat exchanger was a 10 μ filter with a stainless steel housing for ensuring fluid purity. The flow rate was adjusted by a primary control valve which controlled the flow rate to the nozzle, and a bypass valve which routed liquid back to the reservoir. Accurate volumetric flow rate measurement at both low and high flow rates was achieved by means of two rotameters which covered overlapping ranges of 0.145–1.45 gpm and 0.628–6.28 gpm, respectively. The nozzle back pressure was measured with a high accuracy stainless steel dial pressure gauge with a range of 0 to 100 psig. The fluid then entered the spray nozzle, located within the test chamber, and impinged on the heated surface. The flow loop was instrumented with type K thermocouples at the reservoir, heat exchanger, and nozzle inlet.

Test Heater

Based on the findings of earlier investigators, it was decided that the metallic surface be designed to ac-

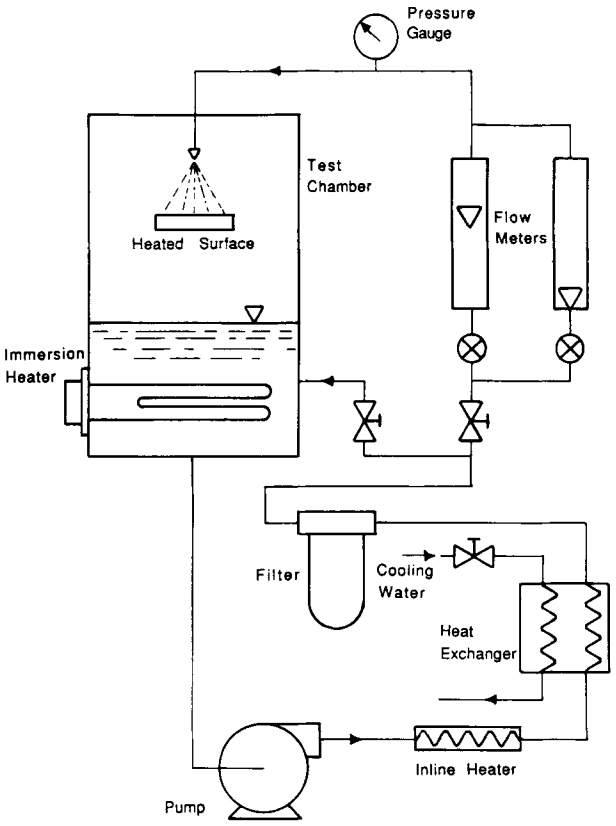

Fig. 3. Schematic of the test facility.

quire heat transfer data using a steady-state technique when possible, and be capable of obtaining accurate local heat transfer measurements. The steady-state technique for obtaining the quench curve consists of electrically heating a spray-cooled metallic surface to maintain steady-state surface termperature for the entire duration of the heat transfer measurements. The heater surface had to be large enough to measure heat transfer rate to sprays with drop diameters up to 3 mm, yet small enough to detect the sharp spatial gradients in the heat transfer coefficient. Since heat transfer from aluminum surfaces was the primary objective of the present study, an initial test heater was constructed of aluminum. Preliminary experiments found the temperature of the heater module much higher than original estimates due to the high fluxes associated with water sprays. Consequently, the aluminum heater used to simulate the quenched surface could not operate at temperatures typical of aluminum forging or extrusion. The aluminum oxidized severely over the time required to take steady-state data, causing some uncertainty in critical heat flux and transition boiling results. Random pitting due to oxidation made characterization of the surface impossible and repeatability of a test highly unlikely.

Based on a study by Baumeister and Simon [17], it was determined that copper and aluminum provide similar boiling heat transfer results due to their high thermal conductivity and nearly isothermal surface conditions. Since some grades of copper are more resistant to oxidation and capable of operating at higher temperatures than aluminum, copper was chosen for heater fabrication.

A copper heater, very similar in construction to the original aluminum heater, was developed to measure local heat transfer rates within the spray field. As shown in Figure 4, the instrumented portion of the heater consisted of a calorimeter bar with a cross-sectional area of 0.5 cm^2. High purity copper was chosen because of its high resistance to oxidation compared to copper alloys, and its nearly constant thermal conductivity of 392 W/m^2K over the operating temperature range of the present study. Heat was supplied to the calorimeter by nine Wattlow Hot Watt cartridge

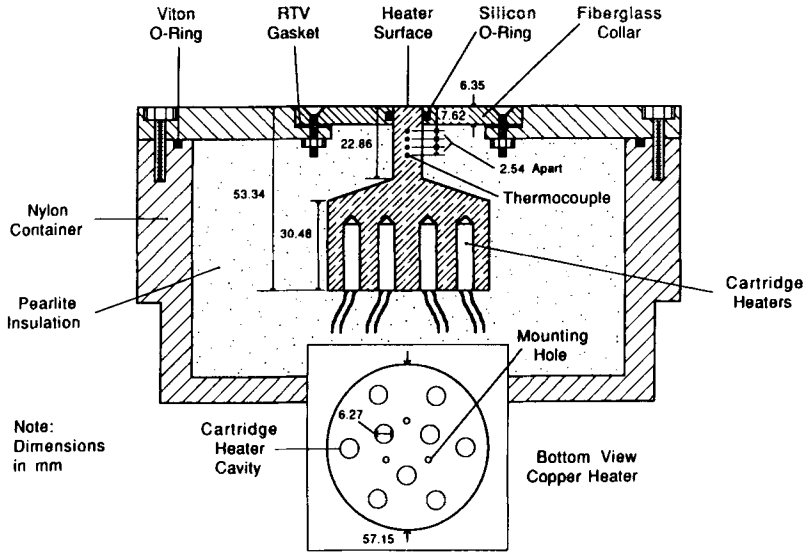

Fig. 4. Construction of the test heater.

heaters rated for 150 W at 120 V and a maximum operating temperature of 760°C. The test heater was designed to achieve a maximum surface heat flux of 900 W/cm^2. Design of the calorimeter section of the heater and surrounding insulation was numerically optimized to ensure one-dimensional heat flow to the quench surface.

The heat flux was determined from the uniform temperature gradient between a series of four chromel-alumel thermocouples spaced 2.54 mm (0.10 in.) apart along the axis of the calorimeter section. Temperature measurements were processed by a Compaq 386 microcomputer used in conjunction with a Keithley 500 data acquisition system. The surface temperature was determined by extrapolating the linear temperature distribution to the surface. The thermocouples, made from 0.0762 mm (0.003 in.) wire, were set along the axis of the calorimeter section through ceramic tubes inserted radially into the calorimeter. The constant cross-sectional area calorimeter section ensured parallel heat flow lines through the thermocouple region. The sample temperature profiles shown in Figure 5 demonstrate the linearity of temperature measurements and support the one-dimensional heat flow assumption.

The heater assembly was mounted on three stainless steel threaded posts which were inserted through ceramic tubes to support the heater inside the heater casing. The casing was constructed from nylon except for the center lid surrounding the quench surface of the calorimeter section, which was fabricated of high temperature G-7 fiberglass. The gap between the heater and the G-7 lid was sealed with a silicone O-ring coated with RTV silicone rubber to achieve a flush surface. At film boiling temperatures, the O-ring became hard and cracked, and the RTV often debonded. Consequently, the seal had to be replaced after every test run.

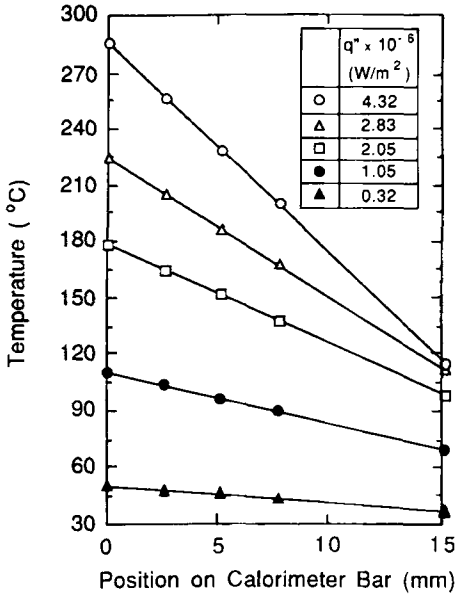

Fig. 5. Typical temperature profiles for heat flux measurements.

Effect of Surface Material

As mentioned in the previous section, Baumeister and Simon [17] showed that a copper heater provides heat transfer results similar to those of an aluminum heater. Figure 6 shows a comparison of results obtained in the present study using aluminum and copper heaters at identical spray conditions. The critical heat flux and transition boiling heat transfer data are only slightly higher for the aluminum heater because of extreme oxidation encountered at prolonged high temperature operation. Oxidation and pitting is believed to enhance CHF and transition boiling by promoting liquid contact with the surface. The rough surface created by oxidation over the course of 2 to 3 hr of testing is not representative of an actual extruded, forged, or cast metallic surface. Thus, it is believed that the CHF results obtained with the oxidation resistant copper heater are more representative of a transient quenching process.

Hydrodynamic Characterization of Sprays

Before the heat transfer characteristics of a spray could be investigated, the local spray parameters such as volumetric spray flux, Q'', drop velocity, u_d, and drop diameter, d, had to be determined. The sprays were then categorized accordingly, and the effects of these parameters on the convection coefficient isolated. The flow parameters were determined for seven stainless

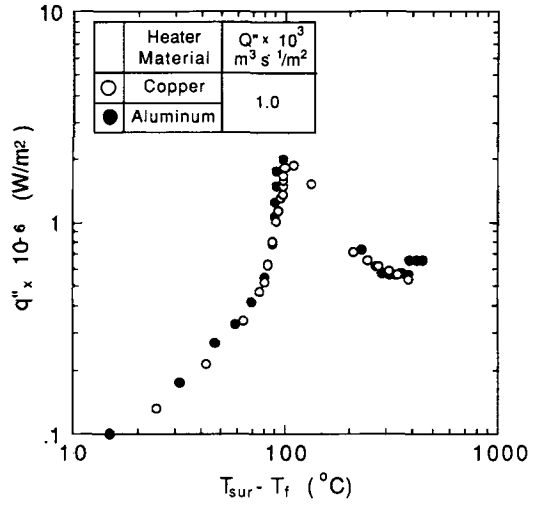

Fig. 6. Comparison of boiling curves obtained by the copper and aluminum heaters.

steel circular solid cone sprays and flat fan sprays. To simplify and reduce the size of the data matrix, all local measurements were limited to the center of each spray.

The water sprays studied were first divided into groups of similar local volumetric spray flux. In order to measure Q'', a 200 ml graduated cylinder with an inlet area of 1.0 cm^2 was constructed. The heater was removed and the cylinder placed in the heater bracket so that the cylinder inlet was at the same location as the test heater. The time required to fill the cylinder was measured, and Q'' was calculated by dividing the volume of water in the cylinder by the fill time and the area of the cylinder inlet. Each nozzle was tested at nozzle-to-plate distances of 10, 15, and 20 in., and nozzle inlet pressures of 10, 20, 40, 60, and 80 psi. By interpolating the results, operating conditions were determined to provide nominal local volumetric spray fluxes of 0.6×10^{-3}, 1.0×10^{-3}, 2.0×10^{-3}, and 10.0×10^{-3} m^3s^{-1}/m^2.

The next step in characterizing the sprays was to measure drop diameters and velocities at the four designated values of Q''. These measurements were obtained by a Two-Dimensional Grey Scale Optical Array Imaging Probe model OAP-2D-GA2 manufactured by Particle Measuring Systems shown in Figure 7. In an Optical Array Probe (OAP), a linear array of photodiodes is illuminated by a laser such that a particle passing through the sampling area casts a shadow on the array, causing a reduction in signal from the array elements shadowed corresponding to the size of the particle.

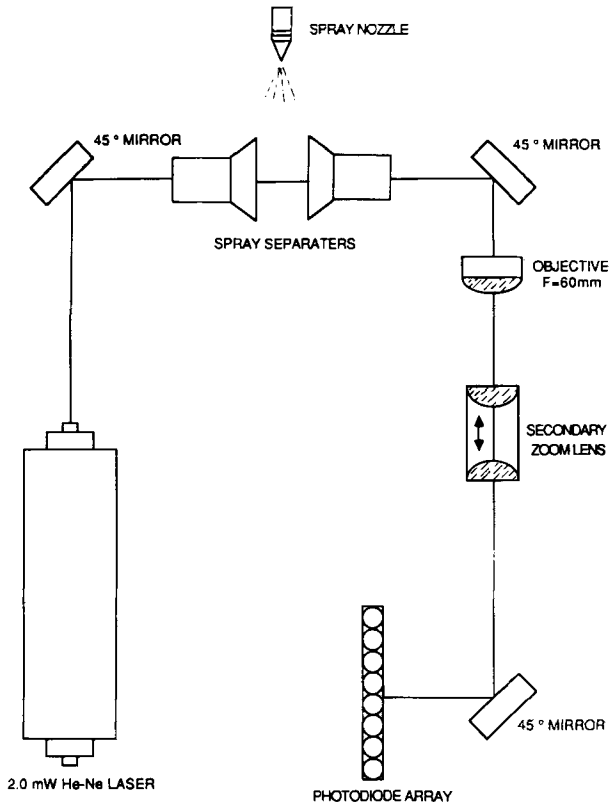

Fig. 7. Optical system diagram for the optical array spectrometer Particle Measuring Systems model OAP-2D-GA2.

Several statistical diameters called mean diameters were calculated at the completion of a particle sampling run. In many calculations of mass transfer and flow processes, it is convenient to work only with mean or average diameters instead of the complete drop size distribution. Mean diameters are desirable because a given spray can be represented by a fictitious spray in which all the drops have the same diameter while retaining relevant characteristics of the original spray. For example, the Sauter Mean Diameter, d_{32}, is the diameter of a drop whose volume-to-surface area ratio is the same as for the entire spray sample. The concept of mean diameter had been generalized and its notation standardized by Mugele and Evans [18]. One of the most popular mean diameters is the Linear Diameter, d_{10}, which is the linear average of all drop diameters in the spray sample. Another diameter commonly used in commercial catalogs to categorize spray nozzles is the Mass Median Diameter, $d_{0.5}$, which is the drop diameter such that 50% of the total liquid volume is in drops of a smaller diameter. A list of some mean diameters and their method of calculation are shown in Table 1. The three mean diameters $d_{0.5}$, d_{10}, and d_{32}, were employed in the present study for characterizing spray performance.

Test Procedure

At the beginning of each test run the system was filled with soft water. The fluid in the system was changed on a daily basis because changes in viscosity over time had a noticeable effect on local volumetric spray flux. The local volumetric spray flux was then measured, as explained previously, and the nozzle height or pressure adjusted until the desired volumetric spray flux was obtained. The test heater was then positioned at the center of the spray field and the copper surface polished with 600 grit wet-dry sandpaper. Power was applied to the heater to bring its surface to a condition within the single-phase heat transfer regime. One hundred temperature readings were recorded every 20 sec. At the end of that interval, readings at each thermocouple location in the calorimeter section and at the nozzle inlet were averaged and saved in a data matrix. These temperatures were then compared to temperatures recorded 1 min and 40 sec earlier. Steady state was assumed if the differences between all corresponding temperatures were less than the convergence criterion of 0.3°C. After steady state was achieved, the power was increased by about 10 W.

Table 1. Mean Diameters and Their Applications (based on Mugele and Evans [18])

Symbol	Name of Mean Diameter	Expression	Application
d_{10}	Linear	$\frac{\Sigma N_i d_i}{\Sigma N_i}$	Comparisons, evaporation
d_{20}	Surface area	$\left[\frac{\Sigma N_i d_i^2}{\Sigma N_i}\right]^{1/2}$	Surface area phenomena e.g. absorption
d_{30}	Volume	$\left[\frac{\Sigma N_i d_i^3}{\Sigma N_i}\right]^{1/3}$	Volume phenomena, e.g., hydrology
d_{21}	Surface diameter	$\frac{\Sigma N_i d_i^2}{\Sigma N_i d_i}$	Adsorption
d_{31}	Volume diameter	$\left[\frac{\Sigma N_i d_i^3}{\Sigma N_i d_i}\right]^{1/2}$	Evaporation, molecular diffusion
d_{32}	Sauter (SMD)	$\frac{\Sigma N_i d_i^3}{\Sigma N_i d_i^2}$	Efficiency studies, mass transfer, reaction
d_{43}	DeBrouckere or Herdan	$\frac{\Sigma N_i d_i^4}{\Sigma N_i d_i^3}$	Combustion equilibrium
$d_{0.5}$	Mass median diameter		

As the surface approached critical heat flux, the power was incremented by only 2 W to determine CHF accurately. The fluid temperature was maintained between 22.5 and 23.5°C throughout the "room temperature" test runs.

Validity of Measurements in Predicting the Quench Curve

Steady-state data were difficult to obtain in the transition and film boiling regimes because of the coupled effect of low surface heat flux and surface oxidation. The low surface heat flux associated with film boiling resulted in slow convergence of temperature readings in the calorimeter bar. However, the surface oxidized rapidly, causing significant change in the heat transfer characteristics. Consequently, before the heater stabilized at a given power setting, the surface changed and the power had to be increased.

In order to obtain accurate data in the film boiling regime for a surface with the same characteristics as the data taken in the single-phase and nucleate boiling regimes, a quasi-steady method was devised to determine heat flux in a relatively short time period. At CHF, the heater temperature slowly increased as transition to film boiling occurred. This increase in temperature occurred at constant electric power input because the surface became partially insulated with a vapor layer. It was discovered, as shown in Figure 8, that the temperature distribution in the calorimeter bar remained one-dimensional as it heated even though the heater was not at steady state. This phenomenon can be explained by the large total heater to quench surface area ratio. As the heat path to the quench sur-

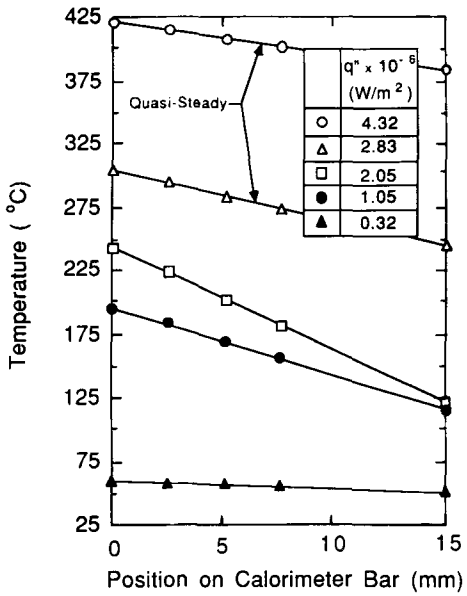

Fig. 8. Steady-State and quasi-steady temperature measurement along the calorimeter bar.

face became less attractive, more heat was lost through the insulation and to the large copper mass below the calorimeter section. This allowed heat flux through the calorimeter bar to remain one-dimensional and provided accurate heat transfer data as surface temperature increased through the transition boiling regime.

The quasi-steady data were compared to many steady-state data before the quasi-steady technique was adopted in the present measurements. Figure 9a shows a comparison of quasi-steady and steady-state data. In the transition boiling region, the steady-state data were slightly higher due to surface oxidation. The quasi-state data were obtained by averaging twenty readings over a 4 sec time interval. Data points were recorded every 20 sec.

The quasi-steady data agreed remarkably well with the steady-state data whether the surface temperature was slowly increasing or decreasing. This is shown in Figure 9b for tests at two different volumetric spray fluxes. For each test, steady-state data were recorded as the power was increased. At $Q'' = 1 \times 10^{-3}$, transition boiling data were also recorded using the quasi-steady method as the surface temperature slowly increased beyond CHF. Once the surface temperature reached 400°C, the surface was allowed to slowly quench by decreasing the electric power input. Quasi-steady data, labeled "quasi-quench" in Figure 9b, were recorded as the surface quenched. The quasi-quench data followed both the steady-state and quasi-steady heating data, demonstrating the reliability of the quasi-steady method and the accuracy of the present measurement techniques in simulating metallic surfaces during quenching by water sprays. However, the quasi-quench data could not capture the peak values at CHF due to the fast transients associated with CHF. Thus, all the CHF data presented in this paper were obtained by the steady-state technique, and use of the quasi-steady technique was limited to the transition and film boiling regimes.

RESULTS AND DISCUSSION

Measurement Uncertainties

Before attempting to interpret the present heat transfer results, it is important to identify the uncertainties associated with the spray data. The atomization of pressure sprays is created by high pressure liquid flow through a small aperture at the tip of a spray nozzle. The liquid jet is disintegrated by the kinetic energy of the liquid itself, resulting in a wide spectrum of drops having different diameters, velocities, and trajectories. This randomness of drop formation makes it impossible to predict drop size, drop velocity, or the number of drops impinging on the surface at any given time. Each nozzle possesses a unique flow field due to undetectable variances in machining. Thus, there is a sizable error associated with using spray flow data from one nozzle to predict heat transfer characteristics of a different nozzle of the same geometry. This problem was eliminated in the present study by using the same nozzle to obtain both the hydrodynamic and heat transfer measurements.

The spray characteristics of most atomizers are also strongly influenced by the fluid properties of density, viscosity, and surface tension. The density of water in the experimental range of the present study was

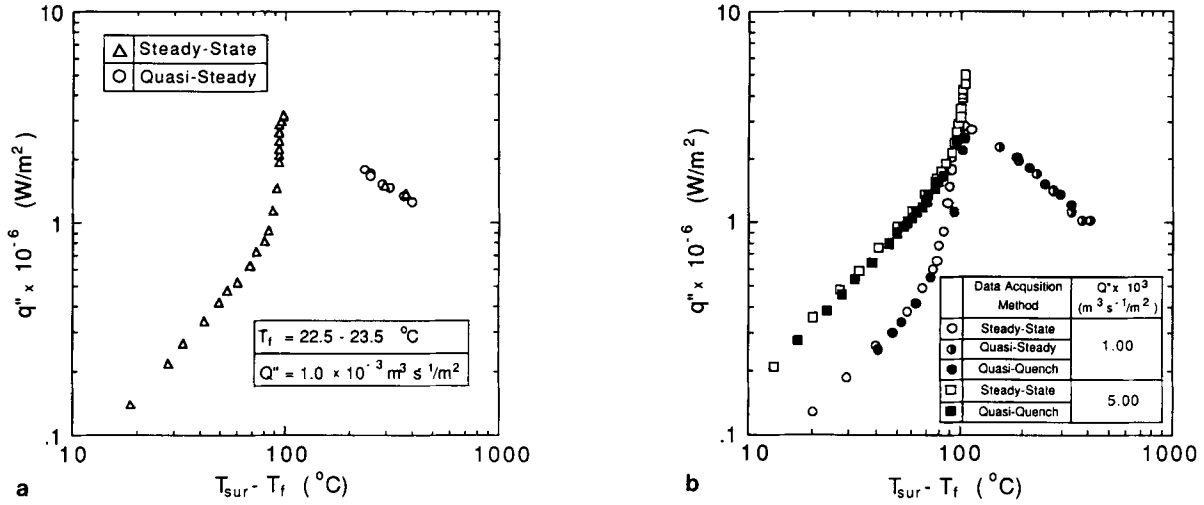

Fig. 9. Comparison of boiling curves obtained using (a) steady-state and quasi-steady techniques and (b) a combination of steady-state, quasi-steady, and quasi-quench techniques.

very stable, but the viscosity and surface tension were susceptible to variation due to entrainment of impurities in the fluid and also to increased fluid temperature. During testing, it was discovered that aging the water 3 days increased the local volumetric spray flux by as much as 20%. The soft water used in the heat transfer studies was continuously filtered and changed daily to minimize the chances of impurities affecting the results. The hydrodynamic measurements, however, were conducted at a separate facility where the fluid was maintained at ambient temperature. Since viscosity resists the growth of instabilities and generally delays the onset of disintegration into drops, as viscosity increases, so does drop diameter. The stability of a drop is also dependent upon surface tension of the fluid. Hence, as surface tension increases, drops in the spray field become larger. Both viscosity and surface tension decrease with fluid temperature; therefore, as the fluid temperature increases, the drop diameters in the spray field become smaller. Since all the hydrodynamic measurements of the present study were performed at ambient temperature, it is expected that the corresponding heat transfer measurements obtained at fluid temperatures above ambient may deviate from the assumed hydrodynamic conditions.

Experimental Results

The first step in characterizing the data was to determine appropriate velocity and length parameters for each spray. Bolle and Moureau [19] outlined a method for calculating the mean velocity of a spray if the drop distribution is known. First, they determined the number, X, of drops crossing a unit transverse surface area per unit time. If the liquid volume flow rate per unit area, Q'', is known, and x_i is defined as the number of drops of diameter d_i crossing a unit area per unit time, then

$$Q'' = \sum_i x_i \left(\frac{\pi d_i^3}{6} \right) \tag{1}$$

where Q'' has the units of velocity. The quantity x_i is proportional to the sample population n_i of drops of diameter d_i determined over an adequate measurement period during which the total number of drops of all sizes is N. That is,

$$\frac{x_i}{X} = \frac{n_i}{N}, \tag{2}$$

where the ratio n_i/N is measured by means of a particle analyzer. At some distance away from the nozzle the momentum flux can be written as $\Sigma_i x_i \rho_f u_{di} (\pi d_i^3/6)$. Thus, the local spray mean velocity, u_m, is defined as

$$u_m = \frac{\sum_i x_i \rho_f u_{di} \left(\frac{\pi d_i^3}{6} \right)}{\sum_i x_i \rho_f \left(\frac{\pi d_i^3}{6} \right)} = \frac{\sum_i (n_i/N) u_{di} \left(\frac{\pi d_i^3}{6} \right)}{\sum_i (n_i/N) \left(\frac{\pi d_i^3}{6} \right)} \tag{3}$$

With this arithmetic mean velocity, the number of drops of diameter d_i are weighted by the volume of a drop of diameter d_i. This mean velocity weighting technique clearly gives more importance to the largest drops.

The characteristic length for a jet is commonly based on the nozzle diameter. However, the nozzle geometry of a spray may not be representative of the spray field downstream from the nozzle. Consequently, a mean drop diameter, such as $d_{0.5}$, d_{10}, or d_{32}, is more practical in characterizing the spray field locally at the position of drop impingement with the heated surface.

Based on the above reasoning, the present correlations were based on characteristic velocities Q'' or u_m, and characteristic mean diameters $d_{0.5}$, d_{10}, or d_{32}.

The flow conditions of the present study are presented in Table 2. Nozzles were chosen that provide similar drop diameter distributions with different mean velocities or similar velocities for different diameters over a volumetric spray flux range of 0.6×10^{-3} to 9.96×10^{-3} m^3s^{-1}/m^2.

The heat transfer results for water sprays impinging on a smooth copper surface of 0.5 cm^2 surface area and a fluid temperature ranging from 22.5 to 23.5°C are shown in Figure 10. Except for the nucleate boiling regime, increasing volumetric spray flux increased the heat flux throughout the boiling curve. Smaller drop diameters increased the single-phase heat transfer coefficient. Increasing mean drop velocity had a noticeable effect of increasing the heat transfer coefficient in the transition region.

The onset of nucleate boiling could not be visually observed even at the lowest spray flux. At $Q'' \leq 2.0 \times 10^{-3}$ m^3s^{-1}/m^2, CHF was easily observed with the naked eye as intermittent dry patches appeared on the surface. As the surface temperature increased beyond CHF, the dry patches became larger and more frequent until the surface was insulated with a large vapor blanket. The transition to film boiling was slow with wetted patches still appearing after CHF even at surface temperatures as high as 225°C. The slow transition to film boiling and high temperature wet patches became more prominent with higher mean spray velocities and smaller drop diameters. At $Q'' = 5 \times 10^{-3}$ m^3s^{-1}/m^2, the transition to film boiling occurred very

Table 2. Data Matrix

Test Number	Spray Type[a]	T_i (°C)	$Q'' \times 10^3$ (m^3s^{-1}/m^2)[b]	P (psi)	$\bar{h}$ (W/m^2K)	$q''_{max} \times 10^{-6}$ (W/m^2)	ΔT_{max} (°C)	u_m (m/s)[b]	d_{10} (mm)[b]	d_{30} (mm)[b]	d_{32} (mm)[b]	d_{43} (mm)[b]	$d_{0.5}$ (mm)[b]
2	45°FC	23	1.04	40	6157	2.41	107	18.6	0.258	0.377	0.544	0.741	0.635
3	45°FC	23	1.00	20	5526	1.87	109	12.9	0.310	0.525	0.878	1.280	1.286
5	15°FC	23	1.05	80	6583	2.85	106	25.2	0.264	0.331	0.405	0.464	0.434
6	30°FC	23	2.02	17	8782	2.84	108	12.1	0.358	0.525	0.760	1.093	0.862
7	45°FC	23	2.02	10	7826	2.52	104	10.9	0.487	0.806	1.351	1.990	2.005
9	45° FC	23	2.00	80	8783	4.23	125	26.7	0.248	0.351	0.485	0.608	0.554
10	15°FC	23	4.99	37	20615	6.38	122	18.1	0.324	0.402	0.491	0.587	0.512
12	30°FC	23	5.0	20	18050	5.84	119	16.5	0.433	0.655	1.160	1.910	1.671
13	30°FC	23	5.0	13.7	16153	5.32	115	14.1	0.366	0.678	1.258	2.011	1.872
14	40°FS	23	5.02	10	17286	6.18	123	11.7	0.481	0.587	0.708	0.850	0.763
17	45°FC	23	0.60	40	4037	1.34	108	16.0	0.257	0.378	0.546	0.730	0.648
18	30°FC	23	9.96	24	23986	—	—	18.8	0.514	0.766	1.208	2.051	1.774
19	45°FC	40	1.07	40	5831	—	—	18.6	0.258	0.377	0.544	0.741	0.635
20	45°FC	60	1.08	40	8021	—	—	18.6	0.258	0.377	0.544	0.741	0.635
21	15°FC	23	0.99	80	—	2.73	104	25.2	0.264	0.331	0.405	0.464	0.434
22	15°FC	30	1.04	80	—	2.77	107	25.2	0.264	0.331	0.405	0.464	0.434
23	15°FC	40	1.08	80	6671	2.70	96	25.2	0.264	0.331	0.405	0.464	0.434
24	15°FC	50	1.10	80	—	2.50	90	25.2	0.264	0.331	0.405	0.464	0.434
25	15°FC	60	1.10	80	7425	2.42	72	25.2	0.264	0.331	0.405	0.464	0.434
26	15°FC	70	1.10	80	—	2.30	62	25.2	0.264	0.331	0.405	0.464	0.434
27	15°FC	80	1.10	80	—	2.15	53	25.2	0.264	0.331	0.405	0.464	0.434
28	30°FC	23	5.06	20	17439	—	—	16.5	0.433	0.655	1.160	1.910	1.671
29	30°FC	40	5.06	20	17615	—	—	16.5	0.433	0.655	1.160	1.910	1.671
30	30°FC	60	5.08	20	18312	—	—	16.5	0.433	0.655	1.160	1.910	1.671

[a]FC ≡ Full cone spray pattern; FS ≡ Flat spray pattern
[b]Hydrodynamic properties of spray determined at T_i = 23°C at the pressure given in the table

rapidly and the oscillations between wet and dry patches could not be observed. Instead, the surface was instantly covered with a vapor blanket and the surface temperature rapidly increased.

The present observations are in agreement with those of Monde [20], who identified two different CHF mechanisms based on volumetric spray flux. He indicated that, for volumetric spray fluxes below 3.0×10^{-3} m^3s^{-1}/m^2, CHF is accompanied by evaporation of all liquid fed to the surface. At volumetric spray fluxes above 3.0×10^{-3} m^3s^{-1}/m^2, on the other hand,CHF occurred in the presence of excess liquid run-off. Monde also noted that transition to film boiling occurred slowly for the low volumetric spray fluxes as the vapor blanket slowly grew in an unsteady manner. At high volumetric spray fluxes, he observed a rapid transition to film boiling.

The data in Figure 10 show that stable film boiling was never obtained for the spray fluxes studied. The boiling curves at the lower spray fluxes start to level off at the upper surface temperature limit of approximately 400°C, suggesting the onset of stable film boiling or the Leidenfrost point. At higher spray fluxes, the Leidenfrost point could not be detected due to the high wall temperature associated with film boiling for these fluxes.

Heat Transfer Correlations

Figures 11a and 11b show single-phase correlations for all the present data including fluid temperatures above ambient. The data are correlated using a Reynolds number based on the Sauter mean diameter or mass mean diameter by the equations

$$Nu_{32} = 2.512\, Re_{32}^{0.76} Pr_f^{0.56} \quad (4)$$

$$Nu_{0.5} = 2.569\, Re_{0.5}^{0.78} Pr_f^{0.56} \quad (5)$$

where all liquid properties are evaluated at $\bar{T} = (T_{sur} + T_f)/2$. Although the typical exponent for Pr_f is 0.35 for most forced convection systems, an empirical exponent of 0.56 was found to provide a more accurate fit. The greatest error occurred with data corresponding to a fluid temperature of 60°C. As previously stated, this may be due to the fact that the hydrodynamic properties of sprays used in the correlation were determined at room temperature instead of 60°C.

The single-phase correlations show no indication of change in slope, suggesting they may hold for a wider range of volumetric spray flux. With this in mind, Figure 12 shows some single-phase heat transfer data obtained for a single stream of drops impinging on an aluminum heater. The linear diameter, d_{10}, was used

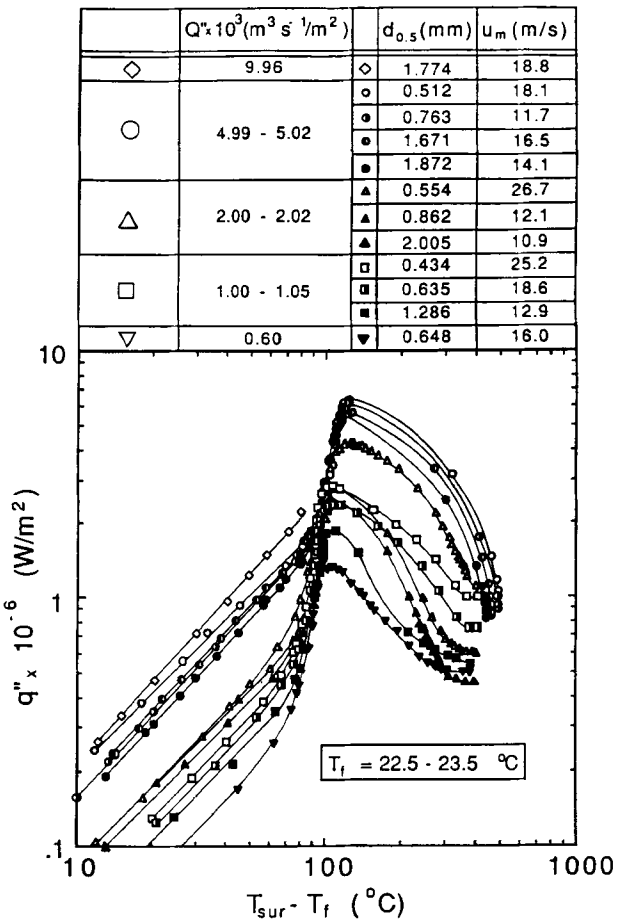

Fig. 10. Spray boiling data.

because it best represents a single drop stream. The single drops were 3.48 mm in diameter compared to a drop diameter range of $d_{10} = 0.248 - 0.487$ mm for the spray data, and impinged on the surface at a rate of 10 drops per sec. Although not enough single drop data have been obtained to provide conclusive evidence, the results suggest the present correlations are applicable to a wide variety of spray conditions.

Figure 13 shows all the nucleate boiling data obtained at a fluid temperature of 22.5 to 23.5°C. While all other regions of the boiling curve seem to be affected by the hydrodynamic properties of the spray, the nucleate boiling regime seems to be dependent only on surface temperature. The data are correlated in the forms

$$q'' = 1.87 \times 10^{-5}(T_{sur} - T_f)^{5.55}, \qquad (6)$$

where q'' is in W/m^2 and $(T_{sur} - T_f)$ in °C. Equation (6) is applicable only for the fluid temperature range shown.

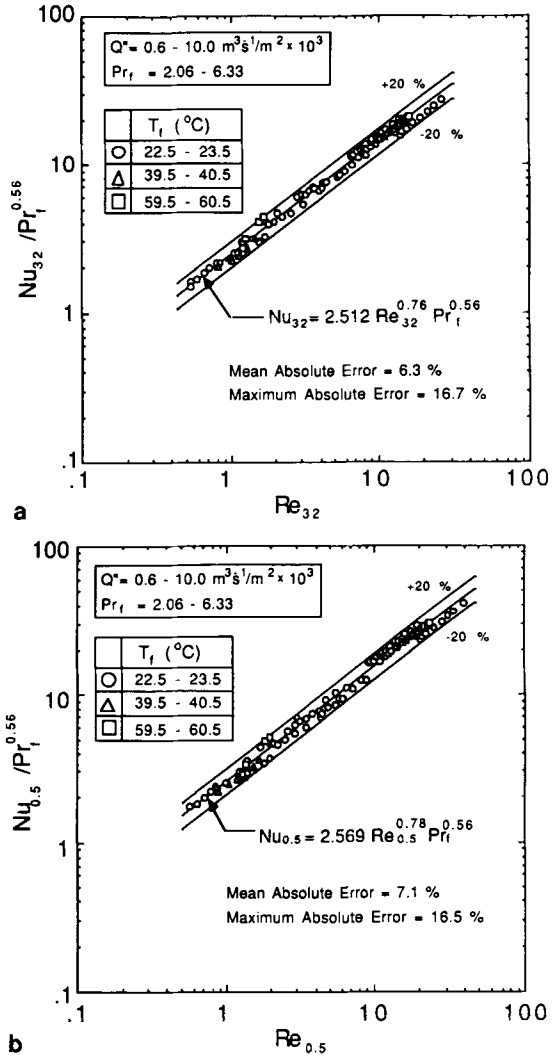

Fig. 11. Single phase correlation based on (a) Sauter mean diameter, d_{32}, and (b) mass mean diameter, $d_{0.5}$.

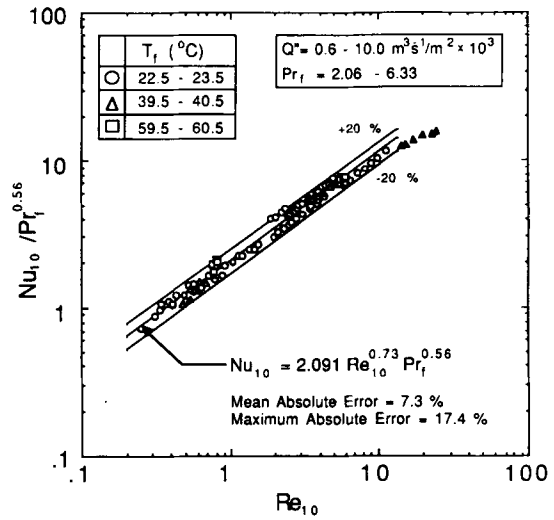

Fig. 12. Single-phase correlation based on the linear diameter d_{10} for spray and single drop data.

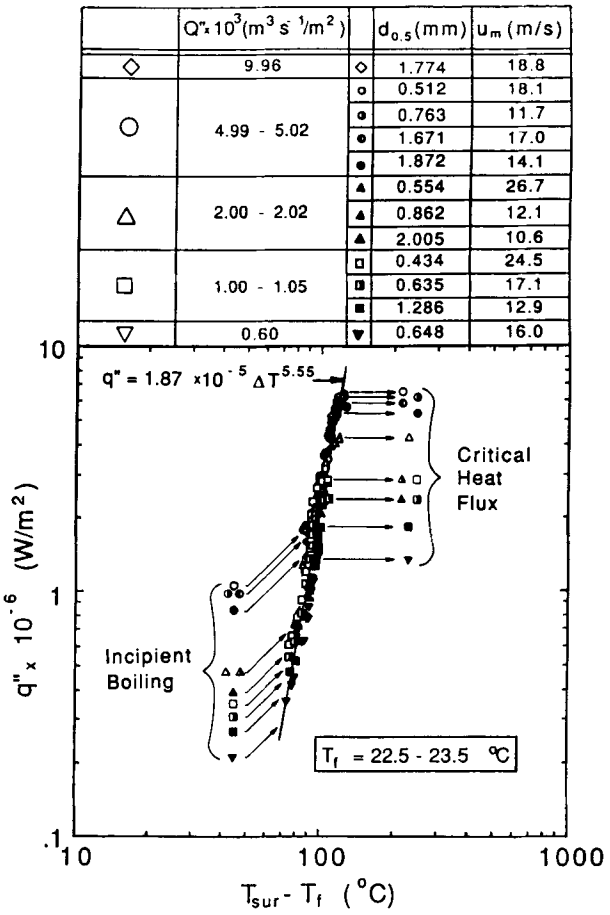

Fig. 13. Correlation of nucleate boiling data for T_f = 22.5 − 23.5°C.

Following the well known correlation technique by Katto [21], CHF data for saturated flow boiling systems can be presented as

$$\frac{q''_{max,sat}}{\rho_g h_{fg} U} = f\left[\frac{\rho_f}{\rho_g}, \frac{\sigma}{\rho_f U^2 L}\right], \tag{7}$$

where U and L are, respectively, the characteristic velocity and length associated with the boiling system. To account for subcooling, Ivey and Morris [22] employed a linear equation of the form

$$\frac{q''_{max}}{q''_{max,sat}} = 1 + C_{sub}\left(\frac{\rho_g}{\rho_f}\right)^{1/4}\left(\frac{\rho_f c_{pf}\Delta T_{sub}}{\rho_g h_{fg}}\right), \tag{8}$$

where $q''_{max,sat}$ is the CHF value for saturated boiling. The Jacob number, $\rho_f c_{pf}\Delta T_{sub}/\rho_g h_{fg}$, in Eq. (8) represents the ratio of sensible heat of a given volume of liquid to the latent heat of an equal volume of vapor. Figure 14 shows a plot of q''_{max} versus fluid subcooling for Q'' = 1.0 × 10^{-3} m^3s^{-1}/m^2. From this data, C_{sub} was empirically determined to be 1.18 × 10^{-2}. Based on Eqs. (7) and (8), the CHF data were correlated with respect to d_{32} and $d_{0.5}$ as shown in Figures 15a and 15b, respectively.

$$\frac{q''_{max}}{\rho_g h_{fg} Q''} = 122.4\left[1 + 0.0118\left(\frac{\rho_g}{\rho_f}\right)^{1/4}\left(\frac{\rho_f c_{pf}\Delta T_{sub}}{\rho_g h_{fg}}\right)\right]\left(\frac{\sigma}{\rho_f Q''^2 d_{32}}\right)^{0.198} \tag{9}$$

$$\frac{q''_{max}}{\rho_g h_{fg} Q''} = 134.3\left[1 + 0.0118\left(\frac{\rho_g}{\rho_f}\right)^{1/4}\left(\frac{\rho_f c_{pf}\Delta T_{sub}}{\rho_g h_{fg}}\right)\right]\left(\frac{\sigma}{\rho_f Q''^2 d_{0.5}}\right)^{0.192} \tag{10}$$

As mentioned in the experimental facility section, it was very difficult to obtain repeatable data in the transition boiling region due to oxidation of the test heater. Nevertheless, an empirical correlation showed significant dependence of transition boiling data on the parameter u_m/Q''. As shown in Figure 16, the Leidenfrost heat flux, nondimensionalized with respect to the superficial vapor velocity, is related to u_m/Q'' by the correlation

$$\frac{q''_{Leid}}{\rho_g h_{fg} Q''} = 0.145\left(\frac{u_m}{Q''}\right)^{0.834}. \tag{11}$$

An empirical correlation of the transition boiling data was established by a polynomial fit to the data starting with the CHF point obtained from Eq. (9). Figure 17a shows significant departure of the data for certain conditions, which can be partially attributed to oxidation effects in these particular experiments. The transition correlation

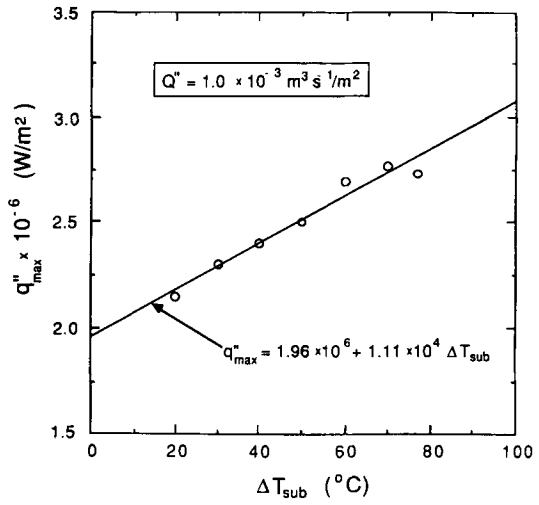

Fig. 14. Variation of CHF with subcooling for Q'' = 1.0 × 10^{-3} m^3s^{-1}/m^2.

$$\log_{10}\left(\frac{q''}{q''_{max}}\right) = 4.78 \times 10^{5}\left(\frac{u_m}{Q''}\right)^{-1.255} \left[\log_{10}\left(\frac{T_{sur} - T_f}{T_{max} - T_f}\right)\right]^{3} - 1.90 \times 10^{4}\left(\frac{u_m}{Q''}\right)^{-0.903} \left[\log_{10}\left(\frac{T_{sur} - T_f}{T_{max} - T_f}\right)\right]^{2} \quad (12)$$

has an absolute mean error of 17%, but a high maximum error of 65%. The critical heat flux, q''_{max}, in Eq. (12) was determined from Eq. (9), and T_{max} was determined by combining Eqs. (6) and (9) and solving

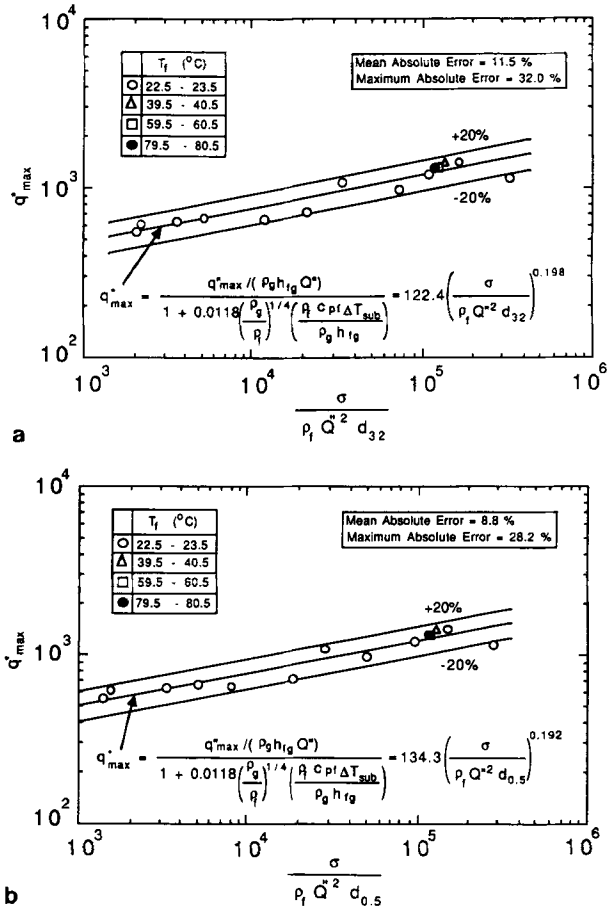

Fig. 15. Correlation of CHF data based on (a) Sauter mean diameter, d_{32}, and (b) mass mean diameter, $d_{0.5}$.

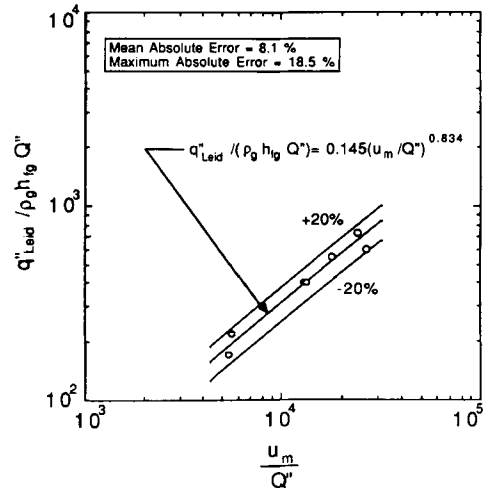

Fig. 16. Correlation of Leidenfrost heat flux data.

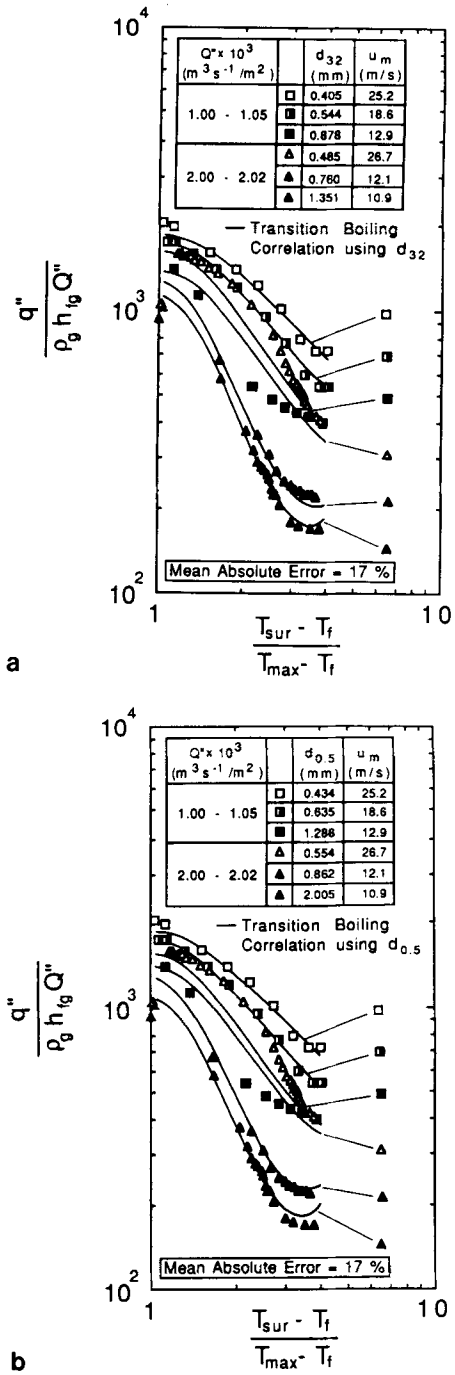

Fig. 17. Correlation of transition boiling data based on (a) Sauter mean diameter, d_{32}, and (b) mass mean diameter, $d_{0.5}$.

for surface temperature. For a fluid temperature of 23°C, this yields

$$T_{max} = 18\left[\left(\frac{\sigma}{\rho_f Q''^2 d_{32}}\right)^{0.198}(\rho_g h_{fg} Q'')\right]^{1/5.55} + T_f. \quad (13)$$

The transition data were reduced in a similar manner using $d_{0.5}$ as the mean diameter, resulting in the correlation

$$\log_{10}\left(\frac{q''}{q''_{max}}\right) = 1.90 \times 10^5\left(\frac{u_m}{Q''}\right)^{-1.144}\left[\log_{10}\left(\frac{T_{sur}-T_f}{T_{max}-T_f}\right)\right]^3 - 1.06 \times 10^4\left(\frac{u_m}{Q''}\right)^{-0.834}\left[\log_{10}\left(\frac{T_{sur}-T_f}{T_{max}-T_f}\right)\right]^2. \quad (14)$$

Table 3. Summary of Correlations

Boiling Regime	Correlation[a]
Single Phase	$Nu_{32} = 2.512\ Re_{32}^{0.76} Pr_f^{0.56}$
	$Nu_{0.5} = 2.569\ Re_{0.5}^{0.78} Pr_f^{0.56}$
Incipient Boiling	$T_{sur} = 13.43\ Re_{32}^{0.167} Pr_f^{0.123}\left(\frac{k_f}{d_{32}}\right)^{0.220} + T_f$
	$T_{sur} = 13.50\ Re_{0.5}^{0.172} Pr_f^{0.123}\left(\frac{k_f}{d_{0.5}}\right)^{0.220} + T_f$
Nucleate Boiling	$q'' = 1.87 \times 10^{-5}(T_{sur} - T_f)^{5.55}$
Critical Heat Flux	$\frac{q''_{max}}{\rho_g h_{fg} Q''} = 122.4\left[1 + 0.0118\left(\frac{\rho_g}{\rho_f}\right)^{1/4}\left(\frac{\rho_f c_{pf}\Delta T_{sub}}{\rho_g h_{fg}}\right)\right]\left(\frac{\sigma}{\rho_f Q''^2 d_{32}}\right)^{0.198}$
	$T_{max} = 18\left[(\rho_g h_{fg} Q'')\left(\frac{\sigma}{\rho_f Q''^2 d_{32}}\right)^{0.198}\right]^{1/5.55} + T_f$
	$\frac{q''_{max}}{\rho_g h_{fg} Q''} = 134.3\left[1 + 0.0118\left(\frac{\rho_g}{\rho_f}\right)^{1/4}\left(\frac{\rho_f c_{pf}\Delta T_{sub}}{\rho_g h_{fg}}\right)\right]\left(\frac{\sigma}{\rho_f Q''^2 d_{0.5}}\right)^{0.192}$
	$T_{max} = 18.3\left[(\rho_g h_{fg} Q'')\left(\frac{\sigma}{\rho_f Q''^2 d_{0.5}}\right)^{0.192}\right]^{1/5.55} + T_f$
Transition Boiling	$\log_{10}\left(\frac{q''}{q''_{max}}\right) = 4.78 \times 10^5\left(\frac{u_m}{Q''}\right)^{-1.255}\left[\log_{10}\left(\frac{T_{sur}-T_f}{T_{max}-T_f}\right)\right]^3 - 1.90 \times 10^4\left(\frac{u_m}{Q''}\right)^{-0.903}\left[\log_{10}\left(\frac{T_{sur}-T_f}{T_{max}-T_f}\right)\right]^2$ based on d_{32}
	$\log_{10}\left(\frac{q''}{q''_{max}}\right) = 1.90 \times 10^5\left(\frac{u_m}{Q''}\right)^{-1.144}\left[\log_{10}\left(\frac{T_{sur}-T_f}{T_{max}-T_f}\right)\right]^3 - 1.06 \times 10^4\left(\frac{u_m}{Q''}\right)^{-0.834}\left[\log_{10}\left(\frac{T_{sur}-T_f}{T_{max}-T_f}\right)\right]^2$ based on $d_{0.5}$
Leidenfrost Heat Flux	$\frac{q''_{Leid}}{\rho_g h_{fg} Q''} = 0.145\left(\frac{u_m}{Q''}\right)^{0.834}$

[a]The dimensions of the parameters used in these correlations are: $q''(W/m^2)$, $d(m)$, $k(W/mK)$, $T(°K)$, $u_m(m/s)$, $Q''(m^3s^{-1}/m^2)$.

As shown in Figure 17b, Eq. (14) has a mean absolute error of 17%.

CONCLUSIONS

An experimental study has been conducted to determine local quenching characteristics for the various regimes in the spray boiling curve. Local measurements of heat transfer to water sprays were made in the single-phase, nucleate boiling, and transition boiling regimes up to surface termperatures of 400°C. Key conclusions from the study are as follows:

1. The volumetric spray flux was found to have a dominant effect on heat transfer compared to other hydrodynamic properties of the spray. However, the effect of drop diameter cannot be neglected when correlating single-phase and CHF data. The mean velocity of the spray, based on the momentum of the drops, was observed to influence the transition regime. Sprays with high mean velocity showed abrupt transition to film boiling.
2. The single-phase heat transfer coefficient was correlated using conventional Nusselt number relations based on Reynolds and Prandtl numbers. These relations were based on the characteristic velocity of volumetric spray flux and a characteristic length of mean drop diameter.
3. The nucleate boiling heat transfer regime was found insensitive to the hydrodynamic properties of the spray. Heat flux data in this regime were correlated as a universal function of the difference between the temperature of the quenched surface and fluid temperature.
4. Critical Heat Flux data were nondimensionalized with respect to Weber number based on volumetric spray flux and mean drop diameter. The subcooling effect was accounted for empirically by employing a linear function of the Jacob number.

A summary of heat transfer correlations obtained for each regime of the spray boiling curve, and of transition conditions between these regimes, is given in Table 3.

ACKNOWLEDGMENT

Financial support for this work was provided through a grant from the Computer Integrated Design, Manufacturing, and Automation Center (CIDMAC) of Purdue University. Messrs. Gerry Dail and William Arthur of ALCOA, and Jerry Hagers, Rudi Schick, Ted Butterfield, and Dr. Verne Dietrich of Spraying Systems Co. are thanked for their technical assistance. In addition, Mr. R.G. Mueller of Mueller Sales, Inc. is thanked for providing stainless steel test nozzles for this study.

REFERENCES

1. T.A. Deiters and I. Mudawar: *J. Heat Treating*, 1989, Vol. 7, No. 1, pp. 9–18.
2. C.J. Hoogendoorn and R. den Hond: *Proc. 5th Int. Heat Transfer Conf.*, 1974, Paper B3.12, Tokyo, pp. 135–138.
3. J.K. Brimacombe, P.K. Agarwal, L.A. Baptista, S. Hibbins, and B. Prabhakar: *63rd National Open Hearth and Basic Oxygen Steel Conf. Proc.*, 1980, Vol. 63, pp. 235–252.
4. L. Bolle, and J.C. Moureau: *Proc. of Two Phase Flows and Heat Transfer*, 1976, Vol. III, NATO Advanced Study Institute, pp. 1327–1346.
5. L. Bolle and J.C. Moureau: *Int. Conf. on Heat and Mass Transfer Metalurgical Processes*, 1979, Dubrovnik, Yugoslavia, pp. 527–534.
6. E.F. Bratuta and S.F. Kravtsov: *Thermal Engineering*, 1986, Vol. 33, pp. 674–676.
7. M. Ishiguro: *Tetsu-to-Hagane'*, 1974, Vol. 60, pp. 464–465.
8. M. Mitsutsuka: *Tetsu-to-Hagane'*, 1968, Vol. 54, pp. 1457–1471.
9. E. Mizikar: *Iron Steel Engineer*, 1970, Vol. 47, pp. 53–60.
10. H. Muller and R. Jeschar: *Arch. Eisenhuttenwes*, 1973, Vol. 44, pp. 589–594.
11. T. Nozaki, J. Matsuno, K. Murata, H. Ooi, and M. Kodama: *Transactions ISIJ*, 1978, Vol. 18, pp. 330–338.
12. U. Reiners, R. Jeschar, R. Scholz, D. Zebrowski, and W. Reichelt: *Steel Research*, 1985, Vol. 56, pp. 239–246.
13. K. Sasaki, Y. Sugitani, and M. Kawasaki: *Testu-to-Hagane'*, 1979, Vol. 65, pp. 90–96.
14. M. Shimada and M. Mitsutsuka: *Tetsu-to-Hagane'*, 1966, Vol. 52, p. 1643.
15. L. Urbanovich, V. Goryainov, V. Sevost'yanov, Y. Boev, V. Niskovskikh, A. Grachev, A. Sevost'yanov, and V. Gur'ev: *Steel in the USSR*, 1981, Vol. 11, No. 3, pp. 184–186.
16. S.C. Yao and K.J. Choi: *Int. J. Multiphase Flow*, 1987, Vol. 13, pp. 1167–1187.
17. K.J. Baumeister and F.F. Simon: *Trans of ASME, J. of Heat Transfer*, 1973, pp. 166–173.
18. R.A. Mugele and H.D. Evans: *Ind. Eng. Chem.*, 1951, Vol. 43, pp. 1317–1324.
19. L. Bolle and J.C. Moureau: *Multiphase Science and Technology*, G.F. Hewitt, J.M. Delhaye, N. Zuber, eds., Vol. 1, pp. 1–93, Hemisphere Pub. Corp., New York, 1973.
20. M. Monde: *Trans. of the JSME*, 1979, Vol. 45, pp. 849–858.
21. Y. Katto: *Proc. of the ASME/JSME Thermal Eng. Joint Conf.*, 1983, Vol. 3, pp. 1–10.
22. H.J. Ivey and D.J. Morris: *U.K. Report AEEW-R-137*, 1962, Winfrith, England.